Trans. Phenom. Nano Micro Scales, 8(2): 109-116, Summer and Autumn 2020
DOI: 0.22111/tpnms.2020.35471.1196

ORIGINAL RESEARCH PAPER

Multi-objective Pareto optimization of frost formation in interrupted Micro Channel Heat Sinks (MCHS) considering microfluidic effects in slip regime

Mostafa Yousefi, Hamed Safikhani*, Homayoun Shabani

Department of Mechanical Engineering, Faculty of Engineering, Arak University, Arak 38156-88349, Iran

Received 22 August 2020; revised 15 October 2020; accepted 15 October 2020; available online 10 November 2020

ABSTRACT: In this paper, by employing the Computational Fluid Dynamics (CFD) and applying the NSGA II algorithm, the multi-objective optimization of frost formation in the interrupted Micro Channels Heat sinks (MCHS) is investigated considering microfluidic effects in slip flow regime. For numerical modeling, basic equations of humid air and frost including continuum, momentum, energy and phase change mechanism are numerically solved and results are compared with reported data and good agreements are observed. Knudsen number (Kn) is changed so that slip flow regime requirement is accomplished. The design variables are geometrical parameters of MCHSc. In the results section, the Pareto front, which simultaneously displays the changes of the heat transfer rate and the frost formation, will be presented, and it will be demonstrated that the Pareto front conveys very important results for the two phase thermal designing of MCHSc. Finally, the multi-objective optimization results computed in this paper are compared with the CFD data and very useful and valuable information is obtained.

KEYWORDS*: CFD; frost formation; MCHS, microchannel; microfluidic; MOO; slip regime.*

INTRODUCTION

Frost formation is a renowned phenomenon in HVAC, aeronautical and refrigeration industries. Frost mounting on the heat exchanger surfaces, causing higher thermal resistance and also it blocks the air path. Both phenomena decrease energy efficiency of the system. Frost naturally is a porous media with packs of the air trapped in the ice matrix. Therefore, it possesses a marked thermal resistance. The presence of frost in the heat exchanger's channels causes pressure drop with narrowing down the path of the air. In the process of the frost formation, humid flows pass coolant surface and mass transfer of steam present in the wet flow to the ice crystals when the air is saturated. This causes thicker frost and higher freezing density. Many researchers already have studied frost formation by numerical and experimental approaches.

Hayashi et al. [1] was one of the pioneers who studied the growth of frost in three different time periods. The first period includes the primary initiation of the ice crystals which is quite short in comparison of the total time period. In this period frost does not grow markedly thick. Moreover, for this phase, it is not a porous media as it can be assumed as ice idols where convection heat and mass transfer are main growth mechanisms and diffusion to the frost sounds trivial. For the second period known as frost growth phase, frost is a porous media where molecular diffusion of the water vapor is dominant. Mass flow of the water vapor contributed in both increasing the density of the frost as well as growing it. Finally, in the complete growth period of the frost, the temperature of the freezing surface reaches to water triple-point temperature.

Therefore, a cyclic process starts where compressed water vapor diffuses through the frost and gradually freezes due to internal temperature gradient.

Aoki et al. [2] thoroughly investigated this phase. Modeling frost formation can be classified in analytical models and computational fluid dynamics (CFD) based models. Analytical models generally assume the growth of the frost in only one direction.

Tao et al. [3-4] proposed a model for mass transfer in frost layer. Lee et al. [5-6] presented a uni-dimensional model for simulating growth in frost density and thickness and also they developed a model for analyzing frost layer and air flow.

Using averaging local volume method Le Gall et al. [7] introduced the relative equilibrium to anticipate frost growth. Na and Webb [8-10] suggested a model based on density of supersaturated water vapor in the frost layer. Yang et al. [11] found an effective model to prognosticate the performance of the fin-tube heat exchanger.

Recently, Hermes et al. [12] developed a mathematical model which could accurately predict the frost thickness with a 10% discrepancy with experimental results.

Kandula [13-14] proposed novel equations for frost over the straight surface and investigated the effect of different ambient parameters on frost characteristics.

✉ *Corresponding Author Email: *h-safikhani@araku.ac.ir*
Tel.: +989120686211; Note. This manuscript was submitted on August 22, 2020; approved on October 15, 2020; published online November 10, 2020.

	Nomenclature		
Kn	Knudsen number	v	Vertical velocity (m s^{-1})
Q	Heat transfer (W)	x	Coordinate (m)
n	Number of domains	y	Coordinate (m)
W	Chip width (m)		**Subscripts**
c	Half of channel width (m)	0	Initial value
a	Half of fin thickness (m)	diff	Diffusing through the frost layer
b	Fin length (m)	a	Air
L	Chip length (m)	ef	Effective
D	Channel width (m)	f	Frost
A	Area (m^2)	i	Ice
c_p	Specific heat capacity (J Kg^{-1} K^{-1})	in	Inlet
D	Mass diffusivity coefficient (m^2 s^{-1})	tot	Total
P	Pressure (pa)		**Greek Symbols**
q_{sub}	Specific heat of sublimation (J Kg^{-1})	λ	Thermal conductivity (W m^{-1} K^{-1})
T	Temperature (℃)	μ	Dynamic viscosity (pa s)
t	Time (s)	ρ	Density (Kg m^{-3})
u	Horizontal velocity (m s^{-1})	ε	Porosity

Micro-channel heat exchangers are very efficient compact exchangers. Their benefit in comparison with fin-tube exchangers includes lower volume and weight and higher efficiency. They also possess lower internal space which decreases refrigeration load of the heat exchanger and potentially decreases the contribution in global warming with lower possible leakage of the refrigerant [15]. Lately, micro-channel heat exchangers are prevalent in HVAC systems. These heat exchangers are increasingly applied in chillers especially thermal pumps where they should work in wet and freezing condition. Shao et al. [16] studied a model with distributed micro-channel heat exchangers used in commercial thermal pumps to analyze the frost over the fin-tube evaporators.

Moallem et al. [17-18] investigated the effect of surface temperature, surface coating and water blockage on the freezing performance of the micro-channel heat exchangers. Surface temperature was more important than surface coating and water blockage over frost growth speed and freezing time. Some other studies focused on the frost-defrost cycle of the heat exchangers which is very vital in designing thermal pump systems. Xia et al. [19] studied five different louvered-fin micro-channel heat exchangers and found that condensed droplets dramatically influence the pressure drop and heat transfer in recurring freezing cycles. Zhang and Hrnjak [20] studied the freezing performance of the micro-channel heat exchangers with parallel-flow parallel-fin (PF2) horizontal flat tubes. In comparison with conventional serpentine fins, the freezing performance was improved which is attributed to the superior permeability of the PF2 heat exchangers. Tso et al. [21] developed a distribution model taking into account the non-uniform distribution of the wall and air temperature in the coil to anticipate dynamic behavior of the finned-tube heat exchanger for both frost and non-frost conditions. Wu et al. [22] studied the frost properties of a micro-channel heat exchanger with louvered-fin and derived the equation for the thickness of the frost.

In recent years, Zhu et al. [23-24] concentrated on increasing thermal transfer through the concept of reconstruction of developed thermal layers. This study included some parallel longitudinal micro-channels with some transverse channels. The transverse channels were used to divide the length of the flow into some independent streams. They found that computed hydraulic and thermal boundary layers were readily improved due to the shorter total length of the divided streams within the micro-channel. It was also reported that the pressure drop and also heat transfer improved in divided micro-channels in comparison with conventional micro-channels. In another similar study Cheng [25] analyzed the flow and heat transfer of a double accumulated micro-channel using some micro-processor. The effect of height of the fin's wall to the height of the micro-channel was examined. They found their superior performance compared to the conventional micro-channels. The evaluation of the 3D micro-channels divided with the transverse micro-pores was followed by Chai et al. [26] using experimental and numerical methods. They found the pressure drop and heat transfer for different conditions and geometries of rectangular walls in transverse micro-pores. Wang and Li [27] numerically simulated flow field in micro-channels with triangular walls in transverse micro-pores. Their parametric studies eventuated in an optimized micro-channel with promising performance. Hajmohammadi et al. [28] investigated the slip regime in microchannel heat sinks with one phase flow. They finally compared the the results with the related results without slip regime.

To achieve the optimal thermal behaviors in MCHS in frost formation, a multi-objective optimization (MOO) approach should be used to discover the best possible design points with appropriate heat transfer and frost formation. NSGA II algorithm is one of the best and most complete

multi-objective optimization algorithms, which will be used in this paper as well.

This algorithm was first proposed by Deb et al. [29], and it has been used in recent years in various engineering-related applications [30-33].

To the best of author's knowledge, there has been no study focusing on the multi-objective optimization of the frost formation in micro channels considering the micro-fluidic effects in slip regime. Therefore, such an issue is the aim of this paper.

MATHEMATICAL MODELING

The details of numerical modeling will be described in this section.

GEOMETRY

The geometry investigated in this paper has been schematically illustrated in Figure 1.

As is shown in this figure, a number of parallel domains have been placed next to each other and formed a MCHS. Since, in this MCHS, the flow field in each computational domain is the same, the governing equations have been numerically solved for one domain and finally, the amount of heat transfer from total MCHS have been multiplied by the number of domains to get the total values.

The total heat transfer for the set of MCHS are computed as follows:

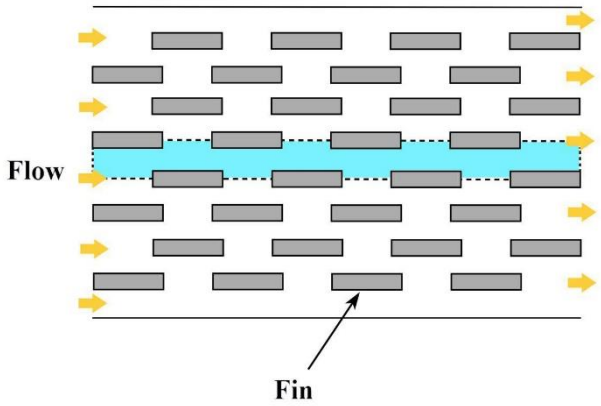

Fig. 1. Schematic view of interrupted MCHS with rectangular fins and the related computational domain

$$Q_{tot} = n\ q_1 \tag{1}$$

$$n = \frac{W}{2(c+2a)} \tag{2}$$

In this paper, the basic dimensions of the MCHS (W and L) are constant and equal to 5 mm, while channel width (D) are 160 μm.

In this way, the examined channels are classified as microchannels. Other design variables are shown in Table 1 and Figure 2.

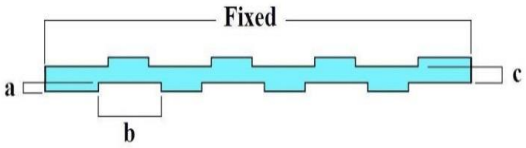

Fig. 2. Geometrical parameters shown in table 1

Table 1
Design variables and their range of variations.

Design variables	From	To
Half of fin thickness (a)	10 μm	30 μm
Fin length (b)	200 μm	275 μm
Half of channel width (c)	60 μm	100 μm

GOVERNING EQUATIONS

In the present CFD modeling it is assumed that humid air is treated as an incompressible Newtonian fluid in laminar flow and density (ρ_a), mass diffusivity coefficient (D_a) and specific heat capacity (c_{pa}) of air are constant. Natural convection is negligible in both humid air and frost. Moreover, the humid air within the frost layer is considered saturated [13]. The continuity, 2D momentum, energy and mass transport equations are as follows:

$$\frac{\partial \rho_a}{\partial t} + \frac{\partial (\rho_a u)}{\partial x} + \frac{\partial (\rho_a v)}{\partial y} = 0 \tag{3}$$

$$\frac{\partial (\rho_a u)}{\partial t} + \frac{\partial (\rho_a u.u)}{\partial x} + \frac{\partial (\rho_a v.u)}{\partial y} = -\frac{\partial P}{\partial x} + \frac{\partial}{\partial x}\left(\mu \frac{\partial u}{\partial x}\right) + \frac{\partial}{\partial y}\left(\mu \frac{\partial u}{\partial y}\right) \tag{4}$$

$$\frac{\partial (\rho_a v)}{\partial t} + \frac{\partial (\rho_a u.v)}{\partial x} + \frac{\partial (\rho_a v.v)}{\partial y} = -\frac{\partial P}{\partial y} + \frac{\partial}{\partial x}\left(\mu \frac{\partial v}{\partial x}\right) + \frac{\partial}{\partial y}\left(\mu \frac{\partial v}{\partial y}\right) \tag{5}$$

$$\frac{\partial (\rho_a T)}{\partial t} + \frac{\partial (\rho_a u.T)}{\partial x} + \frac{\partial (\rho_a v.T)}{\partial y} = \frac{\partial}{\partial x}\left(\frac{\lambda_a}{C_{p,a}} \frac{\partial T}{\partial x}\right) + \frac{\partial}{\partial y}\left(\frac{\lambda_a}{C_{p,a}} \frac{\partial T}{\partial y}\right) \tag{6}$$

$$\frac{\partial (\rho_a w)}{\partial t} + \frac{\partial (\rho_a u.w)}{\partial x} + \frac{\partial (\rho_a v.w)}{\partial y} = \frac{\partial}{\partial x}\left(\rho_a D_a \frac{\partial w}{\partial x}\right) + \frac{\partial}{\partial y}\left(\rho_a D_a \frac{\partial w}{\partial y}\right) \tag{7}$$

For the densification rate of frost layer, the equation proposed by Na and Webb [9] has been used:

$$\frac{\partial (\rho_f T)}{\partial_t} = \frac{\partial}{\partial x}\left(\frac{\lambda_f}{c_{p,f}} \frac{\partial T}{\partial x}\right) + \frac{\partial}{\partial y}\left(\frac{\lambda_f}{c_{p,f}} \frac{\partial T}{\partial y}\right) + \frac{q_{sub}}{c_{pf}} \frac{\partial \rho_f}{\partial t} \tag{8}$$

Using an energy balance for a differential frost volume in the interior of the frost layer, energy equation can be expressed**.**

The viscosity and thermal conductivity are considered temperature dependent. The thermal conductivity of frost is commonly expressed as a function of frost density. In this study, it is used a correlation reported by Lee et al. [6]:

$$\lambda_f \left[{}^{W}/_{(m.K)^{-1}}\right] = A_1 + A_2\rho_f + A_3{\rho_f}^2 \left[\rho \text{ in } {}^{kg}/_{m^3}\right] \quad (9)$$

where $A_1 = 0.132$ $A_2 = 3.13 \times 10^{-4}$ and $A_3 = 1.6 \times 10^{-7}$.

The specific heat is defined as a function of frost density and porosity, as follows:

$$c_{p,f} = \frac{\left(c_{p,f}\rho_g(1-\varepsilon) + c_{p,a}\rho_a\varepsilon\right)}{\rho_f}. \quad (10)$$

The diffusive mass coefficient in the frost layer is determined as Na and Webb [8]:

$$D_{ef} = D_a\varepsilon\frac{1+\varepsilon}{2}. \quad (11)$$

BOUNDARY AND INITIAL CONDITIONS

For numerical simulation, the equations of previous sections should be solved subject to the related boundary and initial conditions.

The schematic subjected boundary conditions are shown in Figure 3.

The fluid entered to the channel with known velocity and temperature (inlet) and exited with the known pressure (outlet). The fins are walls with known temperature lower than freezing temperature.

The slip 1st order boundary conditions (0.001<Kn<0.1) are investigated for walls. This study models the frost layer growth period while the effects of crystal growth period are treated as initial conditions.

Initial frost layer temperature is assumed to be constant and equal to the plate temperature, since the initial thickness is sufficiently thin.

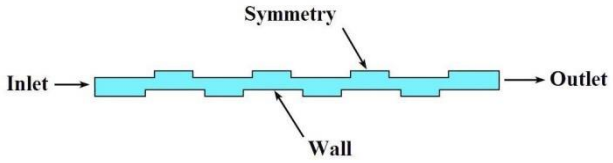

Fig. 3. The boundary conditions used in CFD simulations

NUMERICAL METHODS

The numerical simulation is performed using the finite volume method.

A second order upwind method is used for the convective and diffusive terms and the SIMPLE algorithm is employed to solve the coupling between the velocity and pressure fields.

To make sure that the obtained results are independent of the size and the number of generated grids, several grids with different sizes along different directions has been tested for each MCHS; and it has been attempted to consider for each one the best grid, with the highest accuracy and the lowest computation cost.

A sample of grid generation is shown in Figure 4.

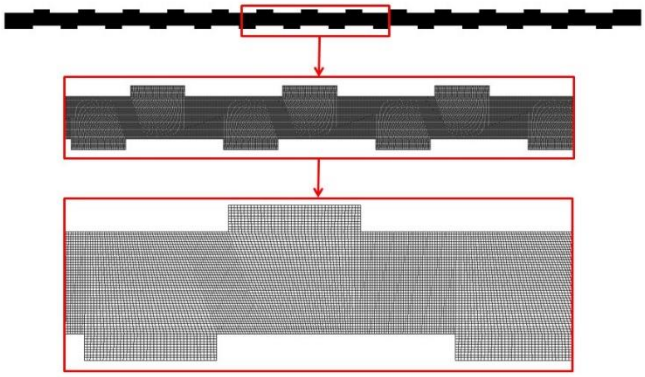

Fig. 4. A sample of grid generations

VALIDATION

To validate the numerical model, its finding is compared with reliable results reported in related references. Since, there is neither experimental nor numerical study available on the frost formation in micro channels considering microfluidic effect in slip regime each frost formation and microfluidic effect should be evaluated separately.

Figure 5a compared the results of frost formation in a conventional macro channel with that CFD data of Wu et al. [34].

As can be seen from Figure 5, present modeling is able to accurately simulate the frost formation.

Similarly, Figure 5b shows the effect of slip effects in a micro-channel developed in this study with that of Hosseini et al. [35] with one phase which reveals great correlation using CFD.

Therefore, it can be said that presented model is accurate and reliable for simulation of frost formation in micro-channels considering microfluidic effects.

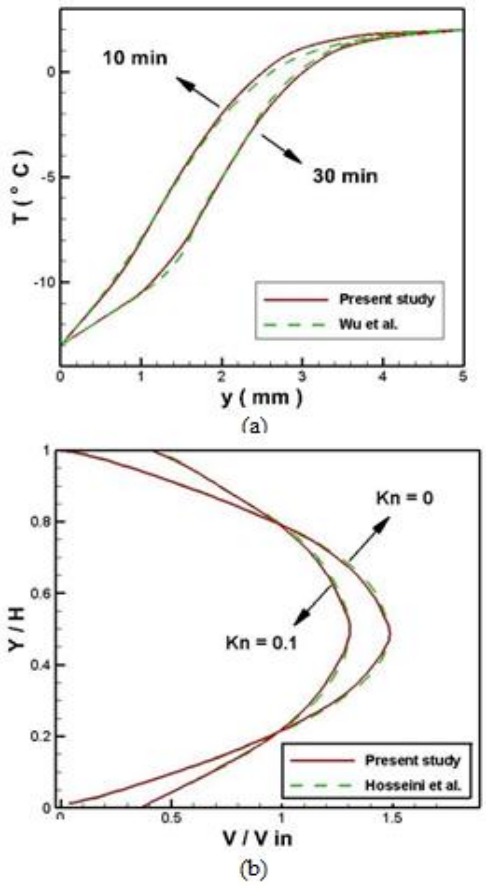

Fig. 5. Validation of frost formation results in a plane [34-35]

Figure 6 shows a sample of CFD contour which shows the frost formation versus relative humidity.

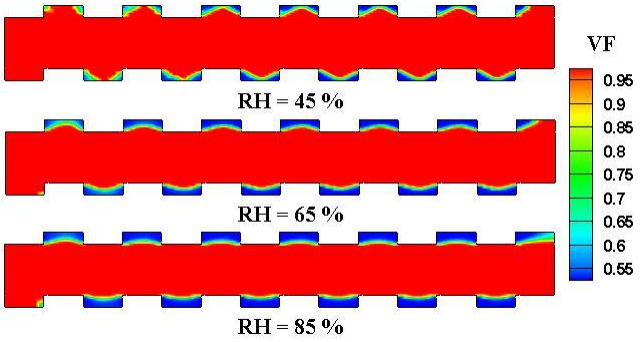

Fig. 6. A sample of Contours of volume fraction versus relative humidity

RESULT AND DISCUSSION

In order to investigate the optimal cooling performance of MCHS, the numerical simulation data were presented in section 2 are now employed in a multi-objective optimization procedure using NSGA II algorithms [29]. In all runs a population size of 60 has been chosen with crossover probability (P_c) and mutation probability (P_m) as 0.7 and 0.07 respectively. The two conflicting objectives are q (heat transfer from MCHS) and VF (volume fraction means the frost formation in MCHS) that should be optimized simultaneously with respect to the design variables (table 1). The multi-objective optimization problem can be formulated in the following form:

$$\begin{cases} Maximize & q = f_1(a,b,c) \\ Minimize & VF = f_2(a,b,c) \end{cases} \tag{12}$$

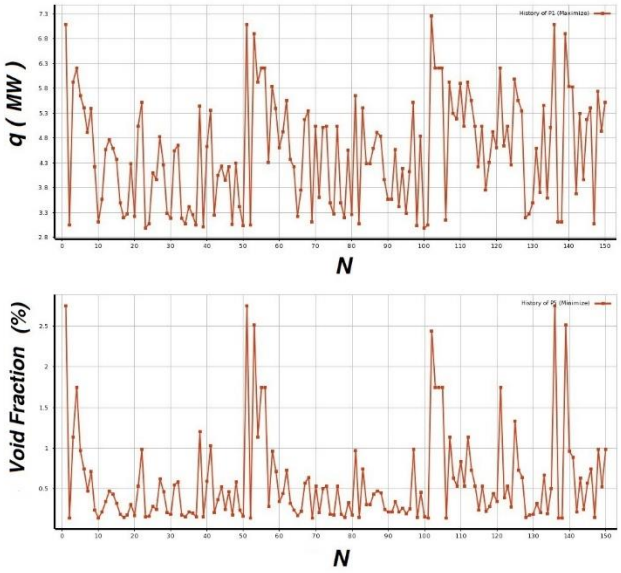

Fig. 7. Samples of CFD data

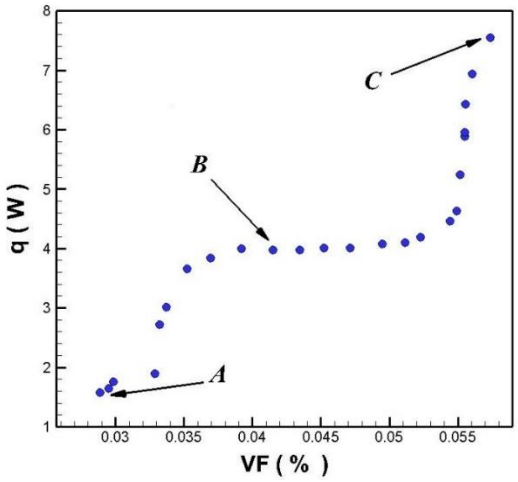

Fig. 8. Pareto front

The results of 200 numerical simulations (200 different sets of MCHS) have been used in the optimization process as shown in Figure 7. Figure 8 shows the Pareto front obtained for the two mentioned objective functions. As this Figure indicates, the points in the Pareto front have no dominancy over one another; i.e., no two points could be found with one of their objective functions equal to each other and another

of their objective functions different from each other. In other words, if we move from one optimal point to another, one objective function will definitely improve and another objective function will certainly get worse. To make an interesting and useful comparison, the optimal data obtained from the Pareto front are compared and illustrated along with the existing CFD data of present study in Figure 9. According to this figure, the Pareto front distinguishes the best boundary of the CFD data which confirms the validity of the multi-objective optimization approach presented in this paper. Although all the points in this Pareto front are optimal points, three points with special and unique characteristics are also observed, which have been designated as Points *A*, *B* and *C*. The details of the design variables, objective function values and some of the other important parameters of these three optimal points have been shown in Table 2. Points *A* and *C* display the best VF and q, respectively.

Table 2
The values of objective functions and the associated design variable of the optimum points

Point	Design Variable			Objective functions		Other important parameters	
	$a\ (\mu m)$	$b\ (\mu m)$	$c\ (\mu m)$	$q_1(MW)$	$VF\ (\%)$	$Q_{total}(MW)$	$n = \frac{W}{2(c+2a)}$
A	10.2	201.0	60.4	1.65	2.9	51.2	31
B	19	209.5	61.4	4.0	4.1	100.2	25
C	23.4	232.7	61.6	7.4	5.7	170.5	23

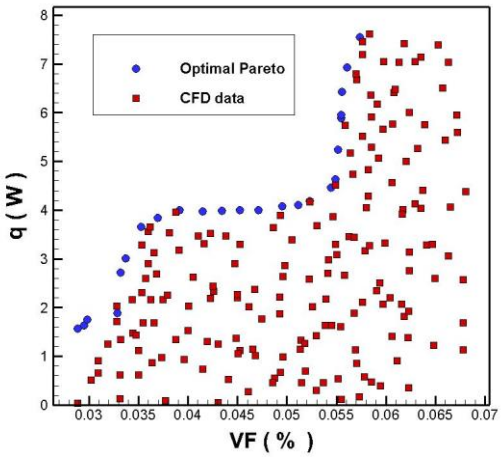

Fig. 9. Overlay of Pareto versus CFD data

In general, an optimal point is a point where both of the objective functions are equally satisfied. In this paper the mapping method [30] is used to compute and find such a point. In this method, both objective functions are mapped between 0 and 1 and then the norm of their sum is calculated. A point with the highest norm is the point at which both objective functions have been optimized to the same value. In this paper, Point *B* has been determined by using the mapping methods, and both objective functions are equally satisfied at this point.

CONCLUSION

In this paper, multi-objective optimization of the frost formation in the interrupted MCHS was investigated considering microfluidic effects in slip flow regime. For numerical modeling, basic equations of humid air and frost including: continuum, momentum, energy and phase change mechanism were numerically solved and results were compared with reported data. Kn number was changed so that slip flow regime requirement was accomplished. This requirement was also considered for setting boundary conditions. The Pareto front, which concurrently illustrates the variations of the frost formation and the amount of heat transfer from the plates, was presented. The Pareto front contains very important information regarding the thermal designing of MCHS subjected to frost formation. By using the Pareto front, three different sets of channels were introduced. In one channel set, the amount of heat transfer is maximized and in the other, the frost formation was maximized. In the third set of channels, both objective functions were equally satisfied. Finally, the multi-objective optimization results computed in this paper were compared with the CFD data and very useful and valuable information was obtained.

REFERENCES

[1] Hayashi Y, Aoki A, Adachi S, Hori K. Study of frost properties correlating with frost formation types. J Heat Transfer. 1977;99:239-45.

[2] AOKI K, KATAYAMA K, HAYASHI Y. A study on frost formation: the process of frost formation involving the phenomena of water permeation and freezing. Bulletin of JSME. 1983;26(211):87-93.

[3] Tao Y-X, Besant R, Rezkallah K. Modeling of frost formation in a fibrous insulation slab and on an adjacent cold plate. International communications in heat and mass transfer. 1991;18(5):609-18.

[4] Tao Y-X, Besant R, Rezkallah K. A mathematical model for predicting the densification and growth of frost on a flat plate. International Journal of Heat and Mass Transfer. 1993;36(2):353-63.

[5] Lee K-S, Kim W-S, Lee T-H. A one-dimensional model for frost formation on a cold flat surface. International Journal of Heat and Mass Transfer. 1997;40(18):4359-65.

[6] Lee K-S, Jhee S, Yang D-K. Prediction of the frost formation on a cold flat surface. International journal of heat and mass transfer. 2003;46(20):3789-96.

[7] Le Gall R, Grillot J, Jallut C. Modelling of frost growth and densification. International Journal of Heat and Mass Transfer. 1997;40(13):3177-87.

[8] Na B, Webb RL. Mass transfer on and within a frost layer. International Journal of Heat and Mass Transfer. 2004;47(5):899-911.

[9] Na B, Webb RL. New model for frost growth rate. International Journal of Heat and Mass Transfer. 2004;47(5):925-36.

[10] Na B, Webb RL. A fundamental understanding of factors affecting frost nucleation. International Journal of Heat and Mass Transfer. 2003;46(20):3797-808.

[11] Yang D-K, Lee K-S, Song S. Modeling for predicting frosting behavior of a fin–tube heat exchanger. International journal of heat and mass transfer. 2006;49(7-8):1472-9.

[12] Hermes CJ, Piucco RO, Barbosa Jr JR, Melo C. A study of frost growth and densification on flat surfaces. Experimental Thermal and Fluid Science. 2009;33(2):371-9.

[13] Kandula M. Frost growth and densification in laminar flow over flat surfaces. International Journal of Heat and Mass Transfer. 2011;54(15-16):3719-31.

[14] Kandula M. Correlation of water frost porosity in laminar flow over flat surfaces. Special Topics & Reviews in Porous Media: An International Journal. 2012;3(1):79-87.

[15] Garimella S. Innovations in energy efficient and environmentally friendly space-conditioning systems. Energy. 2003;28(15):1593-614.

[16] Shao L-L, Yang L, Zhang C-L. Comparison of heat pump performance using fin-and-tube and microchannel heat exchangers under frost conditions. Applied Energy. 2010;87(4):1187-97.

[17] Moallem E, Padhmanabhan S, Cremaschi L, Fisher DE. Experimental investigation of the surface temperature and water retention effects on the frosting performance of a compact microchannel heat exchanger for heat pump systems. International journal of refrigeration. 2012;35(1):171-86.

[18] Moallem E, Cremaschi L, Fisher DE, Padhmanabhan S. Experimental measurements of the surface coating and water retention effects on frosting performance of microchannel heat exchangers for heat pump systems. Experimental Thermal and Fluid Science. 2012;39:176-88.

[19] Xia Y, Zhong Y, Hrnjak PS, Jacobi AM. Frost, defrost, and refrost and its impact on the air-side thermal-hydraulic performance of louvered-fin, flat-tube heat exchangers. International Journal of Refrigeration. 2006;29(7):1066-79.

[20] Zhang P, Hrnjak PS. Air-side performance of a parallel-flow parallel-fin (PF2) heat exchanger in sequential frosting. International journal of refrigeration. 2010;33(6):1118-28.

[21] Tso C, Cheng Y, Lai A. An improved model for predicting performance of finned tube heat exchanger under frosting condition, with frost thickness variation along fin. Applied Thermal Engineering. 2006;26(1):111-20.

[22] Wu J, Ouyang G, Hou P, Xiao H. Experimental investigation of frost formation on a parallel flow evaporator. Applied energy. 2011;88(5):1549-56.

[23] Xu J, Gan Y, Zhang D, Li X. Microscale heat transfer enhancement using thermal boundary layer redeveloping concept. International Journal of Heat and Mass Transfer. 2005;48(9):1662-74.

[24] Xu J, Song Y, Zhang W, Zhang H, Gan Y. Numerical simulations of interrupted and conventional microchannel heat sinks. International Journal of Heat and Mass Transfer. 2008;51(25-26):5906-17.

[25] Cheng Y. Numerical simulation of stacked microchannel heat sink with mixing-enhanced passive structure. International communications in heat and mass transfer. 2007;34(3):295-303.

[26] Chai L, Xia G, Zhou M, Li J, Qi J. Optimum thermal design of interrupted microchannel heat sink with rectangular ribs in the transverse microchambers. Applied Thermal Engineering. 2013;51(1-2):880-9.

[27] Wong K-C, Lee J-H. Investigation of thermal performance of microchannel heat sink with triangular ribs in the transverse microchambers. International Communications in Heat and Mass Transfer. 2015;65:103-10.

[28] Hajmohammadi M, Alipour P, Parsa H. Microfluidic effects on the heat transfer enhancement and optimal design of microchannels heat sinks. International Journal of Heat and Mass Transfer. 2018;126:808-15.

[29] Deb K, Agrawal S, Pratap A, Meyarivan T, editors. A fast elitist non-dominated sorting genetic algorithm for multi-objective optimization: NSGA-II. International conference on parallel problem solving from nature; 2000: Springer.

[30] Safikhani H, Akhavan-Behabadi M, Nariman-Zadeh N, Abadi MM. Modeling and multi-objective optimization of square cyclones using CFD and neural networks. Chemical Engineering Research and Design. 2011;89(3):301-9.

[31] Safikhani H, Hajiloo A, Ranjbar M. Modeling and multi-objective optimization of cyclone separators using CFD and genetic algorithms. Computers & Chemical Engineering. 2011;35(6):1064-71.

[32] Safikhani H, Abbassi A, Khalkhali A, Kalteh M. Multi-objective optimization of nanofluid flow in flat tubes using CFD, Artificial Neural Networks and genetic algorithms. Advanced Powder Technology. 2014;25(5):1608-17.

[33] Amanifard N, Nariman-Zadeh N, Borji M, Khalkhali A, Habibdoust A. Modelling and Pareto optimization of heat transfer and flow coefficients in

microchannels using GMDH type neural networks and genetic algorithms. Energy Conversion and Management. 2008;49(2):311-25.

[34] Wu X, Chu F, Ma Q. Frosting model based on phase change driving force. International Journal of Heat and Mass Transfer. 2017;110:760-7.

[35] Hosseini SMJ, Goharrizi AS, Abolpour B. Numerical study of aerosol particle deposition in simple and converging–diverging micro-channels with a slip boundary condition at the wall. Particuology. 2014;13:100-5.